Springer

KSME

Journal of Mechanical Science and Technology 31 (1) (2017) 123~132
www.springerlink.com/content/1738-494x(Print)/1976-3824(Online)
DOI 10.1007/s12206-016-1211-5

Effects on corrosion resistance of rebar subjected to deep cryogenic treatment †

Srinivasagam Ramesh[1], B. Bhuvaneswari[2], G. S. Palani[2], D. Mohan Lal[1,*] and Nagesh R. Iyer[2]

[1]*Department of Mechanical Engineering, College of Engineering Guindy, Anna University, Chennai - 25, India*
[2]*Structural Engineering Research Centre, CSIR Campus, Chennai-36, India*

(Manuscript Received November 12, 2015; Revised June 7, 2016; Accepted August 3, 2016)

Abstract

An attempt has been made to evaluate the effect of deep cryogenic treatment on the corrosion resistance of rebar. Corrosion behavior of samples subjected to deep cryogenic treatment and samples tempered after deep cryogenic treatment was studied by linear polarization method. The Vickers hardness and ultimate tensile strength of the samples were also measured. The possible mechanism for increase in corrosion resistance has been explained based on Scanning electron micrographs (SEM) and X-Ray diffraction (XRD) study. The morphology of the corroded surfaces of the samples was studied using Atomic force microscopy (AFM). It was found that there is 69 % improvement in corrosion resistance because of deep cryogenic treatment, further it was seen that the increase in corrosion resistance was due to the contribution of increased pearlite phase. Deep cryogenic treatment had no adverse effect on ultimate tensile strength and hardness, which are crucial properties to be considered for rebar.

Keywords: Atomic force microscopy; Corrosion; Cryogenics; Hardness; Linear polarization study; Rebar; Ultimate tensile strength; XRD

1. Introduction

Rebars are used as reinforcement members in Reinforced cement concrete (R.C.C). Rebar is embedded in such a manner that the two materials act together in resisting forces, where tensile and shear stresses are absorbed by the rebar and compressive stress by the concrete. Since rebar acts as a skeleton in reinforced concrete, the performance of rebar is vital. Corrosion leads to volumetric expansion of the steel bars; as we know 'corrosion products' exert compressive pressure on the surrounding concrete of the rebar which leads to development of tensile tension field nearby the interface. Concrete being vulnerable to tensile force results in the formation of cracks from the proximity of the bar to the surface or between the bars. The crack resulted will allow direct exposure of oxygen and moisture to the reinforcement in the concrete which will accelerate the corrosion process and cause spalling of concrete from the surface of the structure [1].

Pantazopoulou et al. [2] suggested that the cracking time was a function of cover, material properties of surrounding concrete and rust product, and was controlled by the rate of rust accumulation. Lundgren [3] modeled the effect of corrosion on bond in the reinforced concrete. He studied the mechanical behavior of the rust which led to the assumption that rust behaves as a granular material and hence its stiffness increases with the stress level. Furthermore, pull-out tests with corroded reinforcement bars suggested a decrease of the bond between the corroded reinforcement and concrete when splitting of concrete occurs. Bhargava et al. [4] formulated a mathematical model to predict the time to cracking of the cover concrete in the corroded reinforced concrete structures considering the combined stiffness of reinforcement, corrosion products and concrete was combined. Shodja et al. [5] formulated a model for the evolution of concrete deterioration due to reinforcement corrosion. The study suggested that the volume fraction of the micro cracks filled with the rust has a vital effect on the predicted time for cracking of the cover and the rate at which rebar is consumed. Kiani et al. [6] formulated a model to predict the penetrated rust into micro cracks of concrete caused by reinforcement corrosion. The study suggests that the variations of the tensile strength of concrete, the density and the chemical components of the corrosion products have the most influence on the variation of the ratio of the corrosion products volume inside the concrete cracks to the volume of the cracks (β). The same researchers have reported the response of reinforced concrete structures to macrocell corrosion of reinforcements before and after propagation of microcracks. The study suggests that the radius of the rebar, the ratio of iron mass to the molecular mass of the corrosion products, mechanical behavior of the rust, the variation of tensile strength and initial elastic modulus of concrete has an influence on the concrete cracking [7, 8]. When corrosion exceeds 12 %, the tensile strength falls below 600 MPa which

*Corresponding author. Tel.: +91 44 22357609
E-mail address: mohanlal@annauniv.edu
† Recommended by Associate Editor In-Ha Sung

is a requirement for rebar as per American Society for Testing and Materials (ASTM) A 615 [9]. Corrosion behavior of rebar is of great concern for durability of concrete structures. Corrosion in rebar occurs due to atmosphere i.e. oxygen during transport and storage or it happens after being embedded in concrete as reinforcement [9-12]. There are mainly two type of corrosion mechanisms taking place on rebars embedded in concrete i.e. microcell and macrocell corrosion. In microcell corrosion anodic and cathodic reactions occur in the rebar proximity with one another, which leads to uniform iron dissolution over the whole surface. In macrocell corrosion there is a net distinction between anodic and cathodic corroding areas [13]. Both macrocell and microcell corrosion have a significant role, and any one of them cannot be overlooked [14]. The total corrosion rate on the actively corroding bar is a summation of macrocell and microcell corrosion components [15]. Studies show that in pre rusted and rust free rebar the corrosion rate can be considered acceptable at low chloride content (< 1 μm/year) but as the chloride content increases above 2.5 % by weight of cement the corrosion rate is unacceptable in both pre-rusted and rust free rebar [16]. Corrosion increases bond strength and contact resistivity at the beginning but as it gets severe the bond strength starts to decrease whereas the contact resistivity keep increasing [17]. Corrosion being a surface phenomenon, in most of the exposure condition, coating of the system provides a solution for corrosion. Hot-dip galvanizing and epoxy coated systems are widely used to minimize the effect of corrosion [18-21].

Barron et al. [22] slowly cooled 316 SS, 410 SS, 4142Cr-Mo, S-2 tool steel and M-1 tool steel down to liquid nitrogen temperature at 2.5 K/min, soaked for 24 hours and allowed to warm up to room temperature in ambient air. A reduction in corrosion was observed for all the materials after cryogenic treatment. S-2 steel showed a reduction in corrosion rate by a factor of 1.786, which is the maximum improvement among the five selected steels, for 410 SS and M-1 corrosion rate reduced by a factor of 1.2, while 316 SS and 4142 Cr-Mo showed the least effect of less than 1.10. Putatunda et al. [23] concluded that reduction of retained austenite in martensite matrix decreases fracture toughness of the material. Das et al. [24] for AISI D2 steel, Zhirafar et al. [25] for 4340 steel, Harish et al. [26] for En 31 steel and Collins et al. [27] for D2 steel reported a reduction of toughness by deep cryogenic treatment. However, Senthilkumar et al. [28] for 4140 steel and Kollmer et al. [29] for 4140 cold-rolled steel reported that toughness of the material had no significant influence by DCT. Zhu et al. [30] investigated the effect of cryogenic treatment on the medium melting point castable alloy and found that cryogenic treatment is an effective procedure in enhancing the corrosion resistance of SDA-II. Investigators of Marshall Space Flight Center studied the potential benefits of cryogenic treatment on aerospace aluminum alloys. The study pointed out that significant improvements were seen in stress corrosion cracking behavior. Minor increase in tensile strength and hardness were noted for parent metal and no significant changes were found in the tensile properties. Akhbarizadeh et al. [31] studied the effect of applying an external magnetic field during the deep cryogenic heat treatment on the corrosion resistance and wear behavior of 1.2080 tool steel. Samples were austenized at 950 °C for 15 minutes and then oil quenched after which samples were divided into five categories as follows 1) one conventional heat treated 2) deep cryogenically treated at -196 °C for a period of 24 hours 3) deep cryogenically treated at -196 °C for a period of 48 hours 4) deep cryogenically treated in the presence of magnetic field of flux density of 0.12 T for a period of 24 hours 5) deep cryogenically treated in the presence of magnetic field of flux density of 0.12 T for a period of 48 hours. All the samples were then tempered at a temperature of 150 °C for a time period of 3 hours. A decreased carbide precipitation was seen in magnetized deep cryogenic treated sample than the usual deep cryogenic treated sample. Corrosion resistance of sample increases with increased carbide precipitation. Wang et al. [32] investigated the effect of deep cryogenic treatment on intergranular corrosion in AISI 304 stainless steel. Samples were sensitized at 650 °C for 2 hours and then air cooled to room temperature. Samples were immersed in liquid nitrogen for a period of 5, 24 and 48 hours. Three sets were immersed before sensitizing and three sets were immersed after sensitizing. Improvement in intergarnular corrosion resistance was seen for deep cryogenic treated samples. Cryogenic treatment has been attempted to reduce corrosion in order to increase the service life of the materials.

The present study deals with an experimental investigation on the corrosion resistance improvement of Fe 500 rebar by Deep cryogenic treatment (DCT). Corrosion test, tensile test and hardness test were made on samples as being crucial mechanical properties of rebar SEM & XRD studies were made to characterize the microstructural changes whereas atomic force microscopy study was done to characterize corrosion products. Hansson et al. [15] reported that the microcell corrosion the primary mechanism for corrosion in rebars. Hence in the present study microcell corrosion is investigated for which single rebar is placed in a corrosive environment.

2. Experimental study

Rebar of 16 mm diameter was procured and then samples of 10 mm length were cut. Optical emission spectroscopy analysis was made and the chemical composition was ascertained, which is tabulated in Table 1. The samples were split into three categories. First set (DCT) was subjected to DCT the second set (DCT+LT) was subjected to DCT followed by tempering at 200 °C for 2 hours and the third set (RAW) was taken for study as it is. The cryogenic treatment involved cooling of the samples from room temperature to -185 °C at 1 °C/min, soaked at -185 °C for 24 hours, and then the temperature was gradually increased at a rate of 0.6 °C/min to reach room temperature in 6 hours. The cryogenic treatment was done in a computer controlled cryogenic processor (CP-200vi, Applied cryogenic, Inc.). Liquid nitrogen was used as

Table 1. Chemical composition of the sample in percentage.

C	Mg	Si	S	P	Ni	Cr	Mo
0.20	0.87	0.19	0.004	0.012	0.01	0.001	0.020

the cooling medium. Tempering was done to the second set of samples, which were tempered immediately after cryogenic treatment.

2.1 Hardness test

The test was conducted as per the ASTM standard designation E 92-82 [33] using a Vickers hardness tester. Hardness test was conducted using Vickers hardness tester-wolpert group. Vickers hardness test was carried out in order to find out the hardness number based on the indentation made by the diamond indenter, in the form of a right pyramid with a square base and an angle of 136^{o} between opposite faces subjected to a load of 1 kgf. The load was applied for a dwell of 15 sec.

2.2 Tensile test

Tensile test was used to determine the ultimate tensile strength and elongation by applying a tensile load to the rebar of 16 mm diameter. The test was conducted as per the ASTM standard designation A370-03a [34]. For this purpose, 9 samples of 500 mm length were prepared for each condition i.e. RAW, DCT & DCT+LT. Three trials were conducted for each test. Tensile test was conducted using fuel instruments & engineers pvt ltd universal testing machine.

2.3 Electrochemical corrosion test

Electrochemical techniques have been used to study the kinetics of corrosion processes. Electrochemical corrosion study is carried out using a three electrode cell assembly. The corrosion resistance of the sample is measured using the ASTM standard designation G3-89 [35]. The samples were polished to a 1200 grit finish followed by polishing using diamond paste on a rotating linen disc, and finished with polishing on a velvet cloth using white kerosene as a coolant. After the polishing process the samples were dipped in a beaker filled with acetone and cleaned in an ultra sonicator bath for 5 min and then cleaned by acetone and deionized water. The specimen is mounted on a teflon specimen holder to expose 1.00 cm^2 area of polished surface to the test solution (electrolyte).

To determine the corrosion behavior, the specimen was studied in 3.5 % NaCl aqueous solution in an Electrochemical work station (Make: Autolab). A saturated calomel electrode is used as reference electrode, Platinum as an auxiliary electrode and test samples were the working electrodes. The reference electrode is connected to the salt bridge which is connected to the Luggin probe. Linear polarization study was conducted (in the range of 200 mv below and above open circuit potential) with a scan rate of 1 mV/ sec. The study was carried out after exposing the samples to the electrolyte for half an hour in order to stabilize the system. This technique allows the determination of the corrosion potential 'E_{corr}' and corrosion current 'I_{corr}' by the Tafel extrapolation method, by carrying out scans in both the positive and negative directions. Based on the 'I_{corr}' values, the corrosion rate of the sample is calculated by an inbuilt software Nova.

2.4 SEM

To reveal the microstructural changes in the specimen, analysis was made using scanning electron microscope. The samples were first polished using emery sheets of various grits followed by polishing using diamond paste on a rotating linen disc, and finished with polishing on a velvet cloth using white kerosene as a coolant. 2 % Nital was used as etchant. After etching, digital micrographs were taken at various regions of the samples under high resolution using SEM (Hitachi 5× to 300000×).

2.5 X-ray diffraction

X-ray diffraction (XRD) measurements were carried out to study the microstructure of the sample as per ASTM standard designation E 975-03 [36]. XRD measurements were conducted with a Bruker D2 phaser diffractometer using Cu-Kα radiation with step size of 0.02, 30 V, 10 mA. 5° to 80° High angle scanning was employed for the study.

2.6 Atomic force microscopy

Atomic force microscopy (AFM) is an imaging technique used to determine topography and other properties of surfaces. The key component of an AFM is a cantilever that bends in response to forces experienced by its tip as it touches another surface. Sample is analyzed by probing the surface with the tip and the interaction between tip and sample is measured. AFM in contact mode scans surface roughness [37].

Roughness due to corrosion products formed on the surface of sample was studied. In the present study the samples were first polished using emery sheets of various grits followed by polishing using diamond paste on a rotating linen disc, finished with polishing on a velvet cloth using white kerosene as a coolant. After that it was corroded in electrochemical cell for 30 minutes and then dried in hot air. The AFM study was made in non-contact mode using XE-70 PARK SYSTEM.

3. Results and discussion

3.1 Microstructure study

The microstructural evaluation was carried out using SEM in order to understand the possible reason for change in corrosion resistance property. The raw sample (Fig. 1) shows pearlite (white phase) in proeutectoid ferrite (dark phase) structure. In DCT (Fig. 2) and DCT+LT (Fig. 3) samples there was an

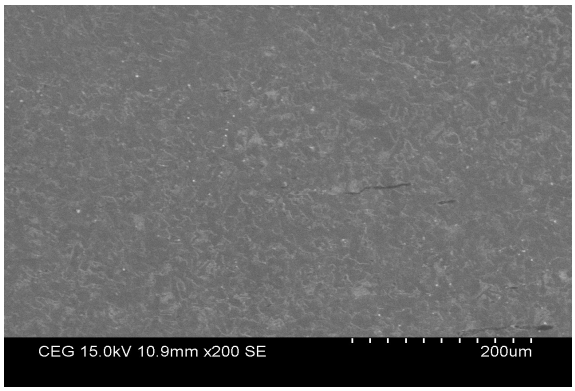

Fig. 1. Microstructure image of raw sample.

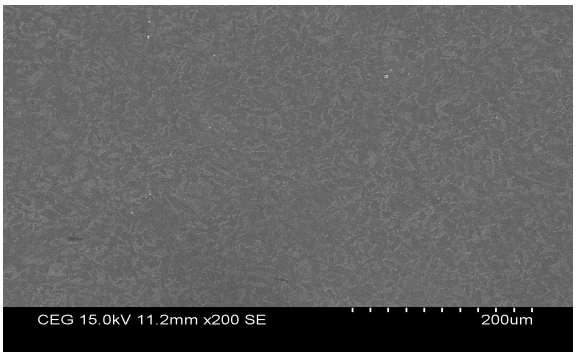

Fig. 2. Microstructure image of DCT sample.

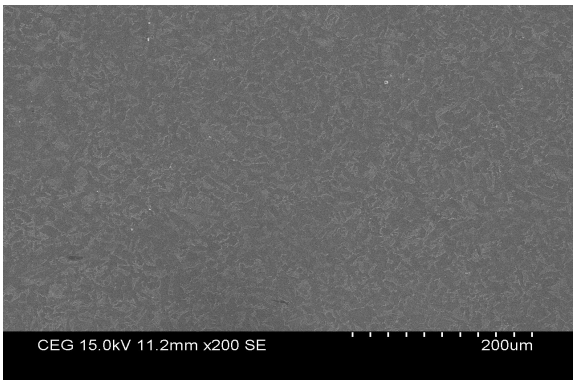

Fig. 3. Microstructure image of DCT+LT sample.

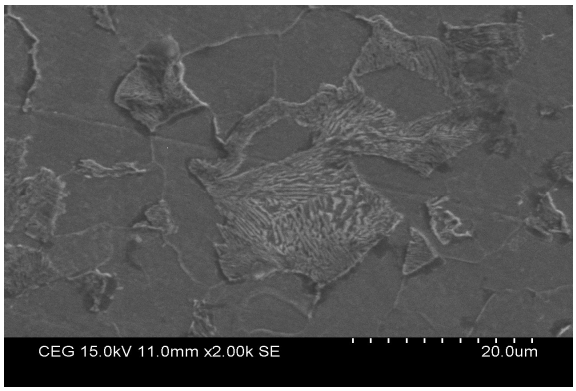

Fig. 4. Microstructure image of RAW sample.

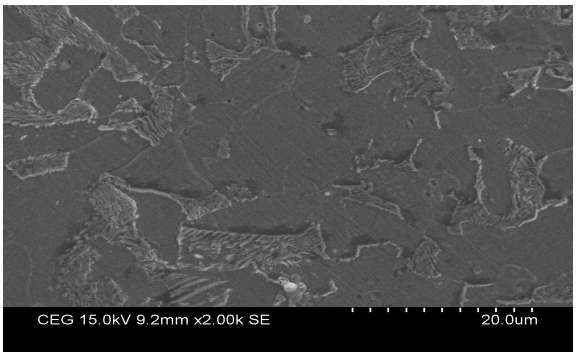

Fig. 5. Microstructure image of DCT sample.

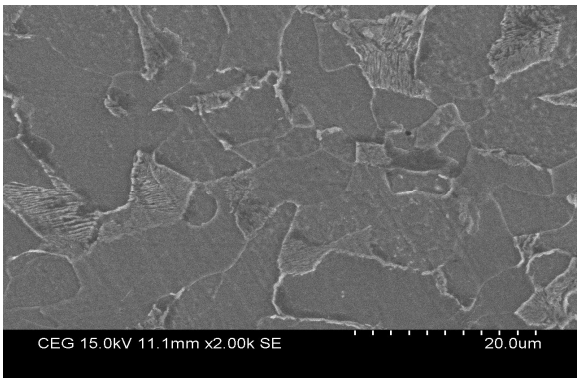

Fig. 6. Microstructure image of DCT+LT sample.

increase in pearlite phase throughout the microstructure in comparison to raw sample. Figs. 4-6 show sample at higher magnification where it can be seen that the microstructure consists of ferrite and pearlite, pearlite shows a mixture of ferrite and cementite in alternative strips in a single grain. Cementite is a very hard intermetallic compound. Cementite being ceramic in nature, exhibit a higher corrosion resistance. Attempts are made by researchers for uniform precipitation of carbides in materials in order to achieve enhanced property [38]. Here uniform precipitation of cementite throughout the structure alternating with ferrite because of DCT can be seen.

SEM images were analyzed using "mgnisci" software to determine pearlite phase fraction and it was seen that RAW samples had 24.71 % pearlite phase whereas in DCT and DCT+LT samples pearlite phase fraction was 40.60 % and 40.16 %, respectively. These observations suggest that there is an increase in pearlite phase uniformly throughout the material in DCT and DCT+LT samples compared to RAW sample. Pearlite when completely dissolved in a matrix results in more stable passivating film and easier passivation [39].

3.2 X-ray diffraction

The diffraction patterns are shown in Fig. 7. The X-Ray dif-

Table 2. Determination of grain size by XRD.

Condition	Grain size (nm)
RAW	32.25
DCT	30.82
DCT+LT	31.18

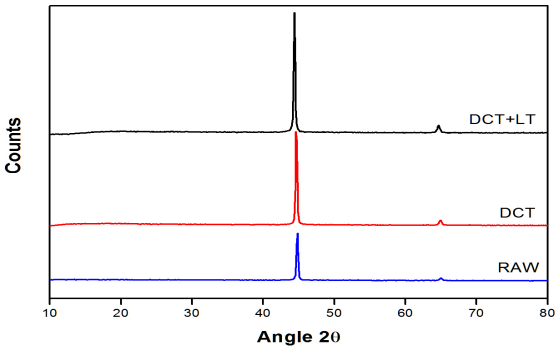

Fig. 7. XRD of RAW, DCT and DCT+LT sample.

fraction study shows that there is an increased α ferrite intensity in DCT & DCT+LT samples when compared to the RAW sample. Further the peak width is broad in DCT & DCT+LT samples in comparison to the RAW sample suggesting that there is a decrease in grain size in DCT & DCT+LT samples which is resulted as an outcome of deep cryogenic treatment made on the rebar sample [40]. The grain size calculated using x-ray difrac software is tabulated in Table 2. Increase in α ferrite intensity might be due to increase in the number of grains as a result of reduced grain size. Further in SEM image increase in pearlite phase was seen for both DCT and DCT+LT samples, so increase in α ferrite intensity is result of increase in both ferrite and pearlite phase.

3.3 Atomic force microscopy

AFM is a powerful technique to investigate the surface roughness. The two dimensional and three dimensional AFM images of polished rebar samples (exposed to 3.5 % NaCl of RAW, DCT and DCT+LT) are shown in Figs. 8-13. Peak profile analysis was also done for the sample which is shown in Figs. 14-16. The Rpv, Rq and Ra value is tabulated in Table 3, for DCT sample roughness was less in comparision to RAW and DCT+LT samples, suggesting that roughness in DCT is less than the other two samples. There is negligible change for RAW and DCT+LT sample. Both RAW and DCT+LT samples have clear peak in the region of -100 nm to 100 nm whereas for DCT the peaks appear in the region of -25 nm to 25 nm.

Results suggest lower roughness value for the surface of DCT samples than RAW & DCT+LT samples. Lower roughness suggests lower and uniform corrosion in the DCT sample which might be due to the lower corrosion rate and decreased & uniform grain size.

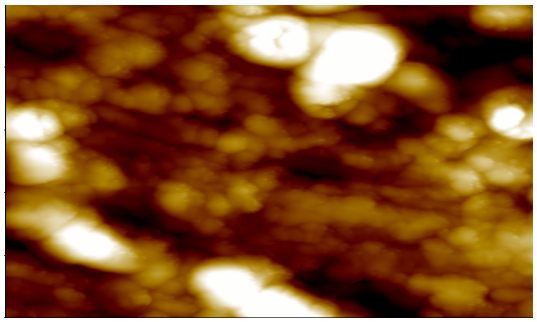

Fig. 8. AFM of RAW sample 2-dimensinal.

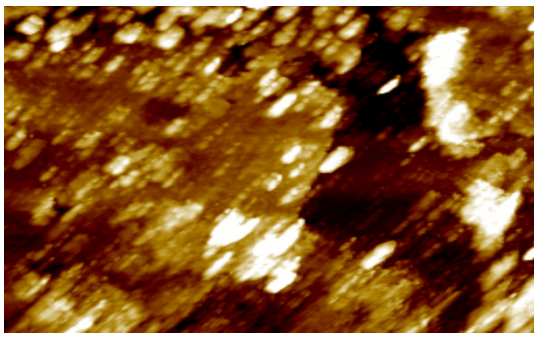

Fig. 9. AFM of DCT sample 2-dimensional.

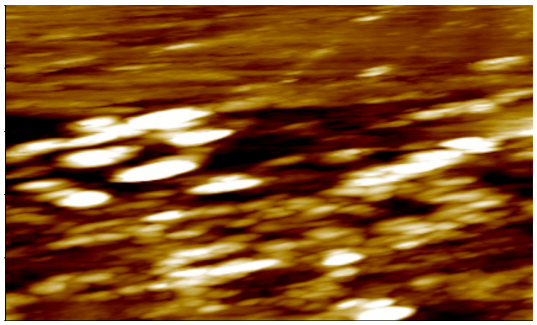

Fig. 10. AFM of DCT+LT sample 2-dimensional.

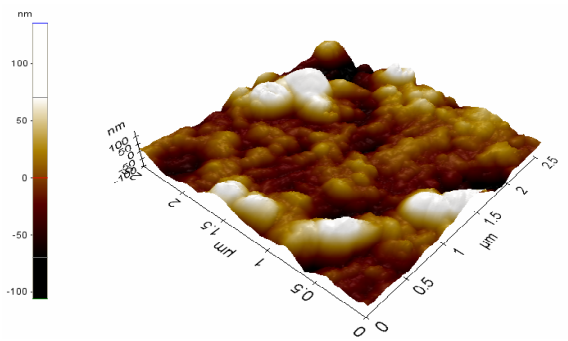

Fig. 11. AFM of RAW sample 3-dimensional.

3.4 Electrochemical corrosion test

To determine the corrosion behavior, linear polarization study was performed on the samples in 3.5 wt. % NaCl aqueous solution. The polarization curves for the rebar are shown

Table 3. Roughness of sample.

Conditions	Rpv	Rq	Ra
RAW	241.237	35.829	27.073
DCT	141.215	9.760	7.455
DCT+LT	397.251	43.017	30.746

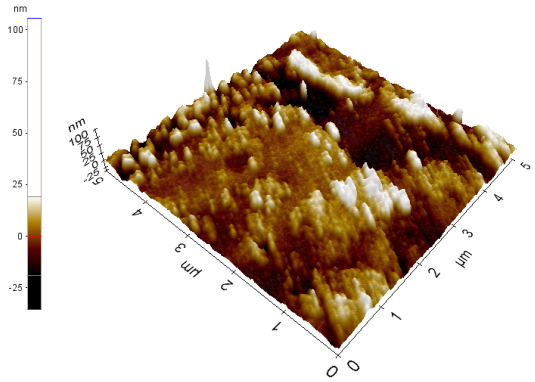

Fig. 12. AFM of DCT sample 3-dimensional.

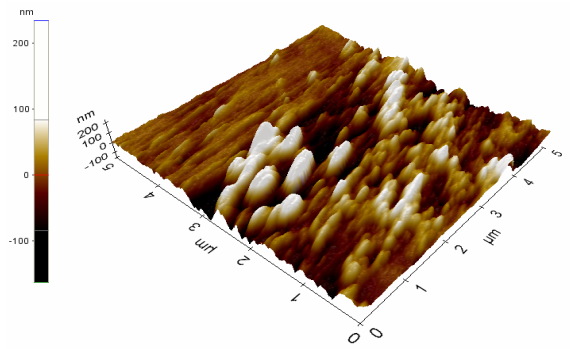

Fig. 13. AFM of DCT+LT sample 3-dimensional.

in Fig. 17. The corrosion potential 'E_{corr}' and corrosion current 'I_{corr}' are determined by the Tafel extrapolation method, by carrying out scans in both the positive and negative directions. Based on the 'I_{corr}' values, the corrosion rate of the sample in electrolyte is calculated and presented in Table 4. It was seen that DCT gave negative 'E_{corr}' value and an 'I_{corr}' value lower than that of the raw sample. Hence an increase in corrosion resistance is observed. Cryogenically treated and tempered steel gave a positive 'E_{corr}' value and an 'I_{corr}' value greater than that of the RAW sample. Hence DCT+LT have reduced corrosion resistance as compared to the raw sample.

The most stable configuration of the metal is its particular crystal lattice, grain boundaries being high-energy areas are more active chemically. Hence, grain boundaries are usually attacked quickly than grain faces when exposed to a corrosive environment [41]. DCT refines and stabilizes the crystal lattice structure and distributes carbide particles throughout the material and all of the individual constituents that make up an alloy are placed in their most stable state. These constituents are aligned uniformly with surroundings [42], resulting in increased corrosion resistance. In DCT samples grain refinement can be seen which reduces the area for the diffusion of NaCl in the metal [22, 40], and thus preventing exposure of the adjacent grains of the microstructure to corrosion. There was a fine precipitation of carbides in DCT samples than that

Table 4. Electrochemical corrosion test results for sample A at RAW, DCT+LT and DCT conditions.

Conditions	I_{corr} (µA)	E_{corr} (mV)	Corrosion rate (mm/y)
RAW	25.5820	-608.980	0.29726
DCT	7.83310	-660.730	0.09102
DCT+LT	27.0440	-606.550	0.31425

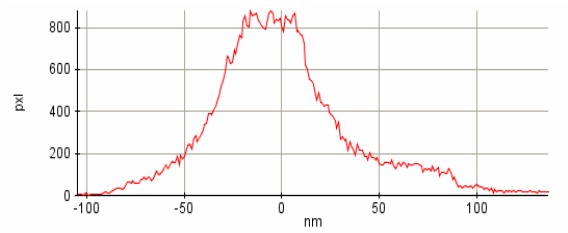

Fig. 14. Peak profile analysis of RAW.

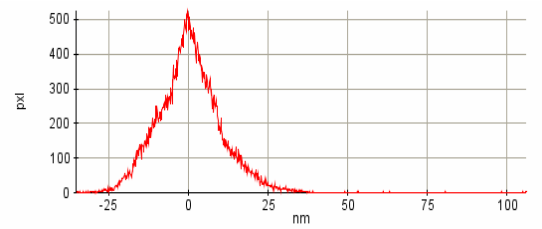

Fig. 15. Peak profile analysis of DCT.

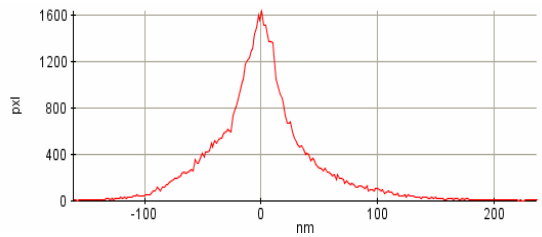

Fig. 16. Peak profile analysis of DCT+LT.

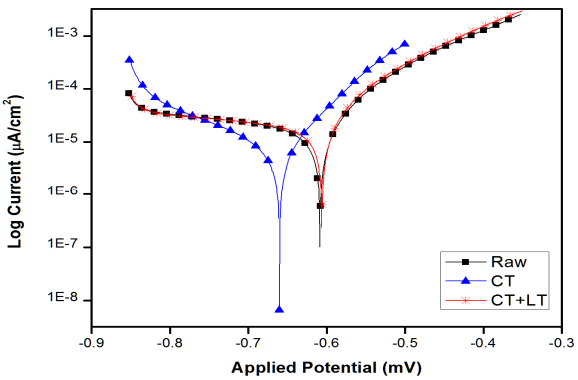

Fig. 17. Tafel curve for RAW, DCT and DCT+LT sample.

of raw samples. It was seen that with increase in carbide precipitation, there was increase in corrosion resistance [31]. The extremely low temperature of cryogenic treatment slows the movement at atomic level which lowers the energy of the system, making it less chemically reactive to the environment. Lower corrosion resistance observed for cryogenically treated and tempered samples was possibly because of the increase in movement in the atomic level which was resulted by the heat supplied during tempering process. When the cementite was oxidized naturally in room temperature, the oxide structure was amorphous and had high corrosion resistance (1-3 wt% NaCl solution). Cementite when oxidized above 400 °C, Fe_3O_4 and α-Fe_2O_3 were formed and had lower corrosion resistance compared to the cementite oxidized naturally [43]. So even though there was carbide precipitation in tempered steel a lower corrosion resistance than DCT has been observed. This suggests that either the temperature of tempering should be brought down or tempering should be excluded in order to maintain a lower energy of the system. Hence result suggest that even though the reduction in microscopic area of grain boundaries, and segregation of carbides has some contribution towards increased corrosion resistance, the key role is played by the lower energy of the system which is an outcome of slow movement at atomic level caused by extremely low temperature of cryogenic treatment and bringing the individual constituent that make up an alloy into their most stable state. Further Cementite oxidized naturally after corrosion gives γ-FeOOH and Fe_3O_4 as corrosion products, which is same as those of the Fe metal. So increase in the volume of corrosion products of DCT samples will be same as RAW and DCT+LT [43]. Hence, DCT will not have any diverse effect on the bond strength between corroded rebar and concrete in comparison to the RAW and DCT+LT samples.

3.5 Hardness test

The results of the hardness test are tabulated in Table 5. It is found that there is only limited increase in hardness value of DCT samples. In the SEM analysis of microstructure it is seen that there is an increase in pearlite fraction. Pearlite is a mixture of ferrite and cementite in alternative strips, Cementite is very hard but when mixed with soft ferrite layers its average hardness is reduced considerably. So even though there is an increase in cementite there is only a little change in its hardness.

3.6 Tensile test

Tensile stress in concrete is absorbed by rebar and so the ultimate tensile strength of the rebar material is crucial for the study. For ductile metals, the tensile strength should be regarded as a measure of the maximum load that a metal can withstand under the very restrictive conditions of uniaxial loading. Similarly, Percentage elongation, the ability of the metal to flow plastically before fracture is an indication of the ductility of the material. The tensile test result is tabulated in Table 6. It is found that DCT samples have 1 % improvement in Ultimate tensile strength 16 % reduction in percentage elongation as compared to RAW samples. However, when DCT samples were tempered the Ultimate tensile strength increased by 0.1 % only and the percentage elongation was reduced by 14 % only as compared to RAW samples.

Table 5. Vickers hardness of sample.

Conditions	Hardness (HV1)
RAW	175.9
DCT	176.8
DCT+LT	174.6

Table 6. Tensile strength of sample.

Conditions	UTS (N/mm^2)	Average	Elongation (%)	Average
RAW	618.10	626.48	21.75	22.75
	630.66		24.25	
	630.68		22.25	
DCT	623.95	633.227	17.12	18.957
	632.34		22.62	
	643.39		17.13	
DCT+LT	629.51	625.24	22.87	19.413
	625.90		16.25	
	621.21		19.12	

4. Conclusions

The Electrochemical corrosion study showed that the corrosion resistance of DCT steel was improved by cryogenic treatment compared to the RAW samples.

- Corrosion rate of DCT sample was 0.09102 mm/y whereas for RAW sample and DCT+LT sample the corrosion rate was 0.29726 mm/y and 0.31425 mm/y, respectively. DCT improves the corrosion resistance while low temperature tempering after DCT reverses the effect of DCT on corrosion resistance. Hence low temperature tempering after DCT is to be avoided.
- The tensile strength got increased by 1 % as a result of DCT. However, it can be concluded that corrosion resistance is improved without losing the tensile strength.
- XRD study shows an increased peak width in DCT and DCT+LT samples than Raw sample which suggests that there is a decrease in grain size. Cryogenic treatment has an effect of reducing grain size of material, which has a positive influence on the mechanical properties.
- AFM study shows reduced roughness and uniform corrosion as a result of DCT. Hence it is concluded that reduced grain size due to DCT has the effect of lowering the corrosion rate.
- The present study suggests that the DCT has increased

pearlite phase in the microstructure, which has increased corrosion resistance without affecting the tensile strength of the material and bond strength between rebar and concrete. Hence, DCT is more influential than RAW and DCT+LT in improving corrosion resistance.

The study confirmed that cryogenic treatment is effective in enhancing corrosion resistance property of rebar used in R.C.C.

As such this approach has no drawback if the treatment is done in a precisely controlled cryogenic chamber. However, the additional cost is a point to be considered which will be in terms of initial cost of the treatment chamber for accommodating long rebars and running cost towards liquid nitrogen.

Acknowledgment

The authors would like to express their thanks to the DST-FIST & DST-PURSE for providing funds towards the procurement of the Cryogenic chamber and liquid nitrogen, respectively.

We thank Director, CSIR- SERC, for permitting us to conduct electrochemical studies.

Nomenclature

SEM : Scanning electron microscope
XRD : X-ray diffraction
AFM : Atomic force microscopy
DCT : Deep cryogenic treatment
DCT+LT : Low temperature tempering after deep cryogenic treatment
β : Ratio of the volume of the rust penetrated into the microcracks to the total volume of the microcracks
R.C.C. : Reinforced cement concrete
ASTM : American society for testing and materials
E_{corr} : Corrosion potential in mV
I_{corr} : Corrosion current density in μA/cm^2
R_a : Average roughness in nm
R_q : Root mean square roughness in nm
R_{pv} : Peak to valley roughness in nm
UTS : Ultimate tensile strength in N/mm^2

References

[1] I. L. Al-Qadi, J. E. Peterson and R. E. A. Weyers, Time to cracking model for critically contaminated reinforced concrete structures, *Proc. Fifth Int. Conf: on Structural Faults and Repair*, Edinburgh, UK (1993) 91-98.

[2] S. J. Pantazopoulou and K. D. papoulia, Modeling cover-cracking due to reinforcement corrosion in RC structures, *J. Eng. Mech.*, 127 (4) (2001) 342-351.

[3] K. lundgren, Modelling the effect of corrosion on bond in reinforced concrete, *Mag. Concr. Res.,* 54 (3) (2002) 165-173.

[4] K. Bhargava, A. K. Ghosh, Y. Mori and S. Ramanujam, Modeling of time to corrosion-induced cover cracking in reinforced concrete structures, *Cem. Concr. Res.,* 35 (2005) 2203-2218.

[5] H. M. Shodja, K. Kiani and A. Hashemian, A model for the evolution of concrete deterioration due to reinforcement corrosion, *Math. Comput. Modell*., 52 (2010) 1403-1422.

[6] K. Kiani and H. M. Shodja, Prediction of the penetrated rust into the microcracks of concrete caused by reinforcement corrosion, *Appl. Math. Modell.,* 35 (2011) 2529-2543.

[7] K. Kiani and H. M. Shodja, Response of reinforced concrete structures to macrocell corrosion of reinforcement, Part I: Before propagation of microcracks via an analytical approach, *Nucl. Eng. Des.,* 241 (2011) 4874-4892.

[8] K. Kiani and H. M. Shodja, Response of reinforced concrete structures to macrocell corrosion of reinforcement. Part I: After propagation of microcracks via a numerical approach, *Nucl. Eng. Des.,* 242 (2012) 7-18.

[9] A. A. Almusallam, Effect of degree of corrosion on the properties of reinforcing steel bars, *Construct Build Mater.*, 15 (8) (2001) 361-368.

[10] E. Zitrou, J. Nikolaou, P. E. Tsakiridis and G. D. Papadimitriou, Atmospheric corrosion of steel reinforcing bars produced by various manufacturing processes, *Construct Build Mater.*, 21 (2007) 1161-1169.

[11] V. Kumar, Protection of steel reinforcement for concrete-A review, *Corros. Rev.,* 16 (4) (1988) 317-358.

[12] B. Elsener, Corrosion rate of steel in concrete-measurements beyond the Tafel law, *Corros. Sci.,* 47 (2005) 3019-3033.

[13] B. Elsener, Macrocell corrosion of steel in concrete - implications for corrosion monitoring, *Cement Concrete Comp,* 24 (2002) 65-72.

[14] S. Qian, J. Zhang and D. Qu, Theoretical and experimental study of microcell and macrocell corrosion in patch repairs of concrete structures, *Cement Concrete Comp,* 28 (2006) 685-695.

[15] C. M. Hansson, A. Poursaee and A. Laurent, Macrocell and microcell corrosion of steel in ordinary Portland cement and high performance concretes, *Cement Concrete Res*, 36 (2006) 2098-2102.

[16] P. Novak, R. Mala and L. Joska, Influence of pre-rusting on steel corrosion in concrete, *Cement Concrete Res*, 31 (2001) 589-593.

[17] X. Fu and D. D. L. Chung, Effect of corrosion on the bond between concrete and steel rebar, *Cement Concrete Res*, 27 (12) (1997) 181l-1815.

[18] O. Kayali and S. R. Yeomaus, Bond of ribbed galvanized reinforcing steel concrete, *Cem. Concr Comp*, 22 (2000) 459-467.

[19] A. U. Malik, I. Andijani, S. Ahmed and A.-M. Fahd, Corrosion and mechanical behavior of fusion bonded epoxy (FBE) in aqueous media, *Desalination*, 150 (3) (2002) 247-254.

[20] A. B. Darwin and J. D. Scantlebury, Retarding of corrosion processes on reinforcement bar in concrete with an FBE coating, *Cem Concr Comp*, 24 (1) (2002) 73-78.

[21] S. Erdogdu, T. W. Bremner and I. L. Kondratova, Accelerated testing of plain and epoxy-coated reinforcement in simu-

lated seawater and chloride solutions, *Cem Concr Res,* 31 (6) (2001) 861-867.
[22] R. F. Barron and R. H. Thompson, Effect of cryogenic treatment on corrosion resistance, *Advances in Cryogenic Engineering Materials*, 36 (1990) 1375-1379.
[23] S. K. Putatunda, Fracture toughness of a high carbon and high silicon steel, *Mater. Sci. Eng. A,* 297 (2001) 31-43.
[24] D. Das, R. Sarkar, A. K. Dutta and K. K. Ray, Influence of sub-zero treatments on fracture toughness of AISI D2 steel, *Mater. Sci. Eng. A*, 528 (2010) 589-603.
[25] S. Zhirafar, A. Rezaeian and M. Pugh, Effect of cryogenic treatment on the mechanical properties of 4340 steel, *J. Mater. Process. Technol*, 186 (2007) 298-303.
[26] S. Harish, A. Bensely, D. M. Lal, A. Rajadurai and G. B. Lenkey, Microstructural study of cryogenically treated En31 bearing steel, *J. Mater. Proc. Technol.,* 209 (2009) 3351-3357.
[27] D. N. Collins and J. Dormer, Deep cryogenic treatment of a D2 cold-worked tool steel, *Heat Treat. Met.*, 24 (3) (1997) 71-74.
[28] D. Senthilkumar, I. Rajendran, M. Pellizzari and J. Siiriainen, Influence of shallow and deep cryogenic treatment on the residual state of stress of 4140 steel, *J. Mater. Process. Technol.,* 211 (2011) 396-401.
[29] K. P. Kollmer, Applications & developments in the cryogenic processing of materials, *The Technology Interface. Electronic Journal for Engineering Technology*, 3 (1) (1999).
[30] Z. Zhu, J. Zhao and X. Huang, Effects of cryotreat on the corrosion resistance of the medium melting point castable alloy, *West China Journal of Stomatology*, 20 (5) (2002) 316-319.
[31] A. Akhbarizadeh, K. Amini and S. Javadpour, Effects of applying an external magnetic field during the deep cryogenic heat treatment on the corrosion resistance and wear behavior of 1.2080 tool steel, *Mater Design*, 41 (2012) 114-123.
[32] Q.-Q. Wang, W.-Z. Wang, F.-Z. Xuan and S.-T. Tu, A new method improving intergranular corrosion resistance of AISI 304 stainless steel, *FM2008 - Evaluation, Inspection and Monitoring of Structural Integrity* (2008) 411-416.
[33] ASTM standard E92-82, Standard test method for Vickers hardness of metallic materials, *Annual book of standards* (2004).
[34] ASTM standard A370-03a, Standard Test Methods and Definitions for Mechanical Testing of Steel Products, *Annual book of standards* (2004).
[35] ASTM standard G3-89, Standard Practice for Conventions Applicable to Electrochemical Measurements in Corrosion Testing, *Annual book of standards* (2004).
[36] ASTM standard E975-03, Standard Practice for X-Ray Determination of Retained Austenite in Steel with Near Random Crystallographic Orientation, *Annual book of standards* (2004).
[37] R. Abedinzadeh, S. M. Safavi and F. Karimzadeh, A study of pressureless microwave sintering, microwave-assisted hot press sintering and conventional hot pressing on properties of aluminium/alumina nanocomposite, *Journal of Mechanical Science and Technology*, 30 (5) (2016) 1967-1972.
[38] A. Kamboj, S. Kumar and H. Singh, Burr height and hole diameter error minimization in drilling of AL6063/15%/SiC composites using HSS step drills, *Journal of Mechanical Science and Technology*, 29 (7) (2015) 2837-2846.
[39] M. Ferhat, A. Benchettara, S. E Amara and D. Najjar, Corrosion behaviour of Fe-C alloys in a sulfuric medium, *J. Mater. Environ. Sci.,* 5 (4) (2014)1059-1068.
[40] J. Mazur, Investigation on austenite and martensite subjected to very low temperatures, *Cryogenics*, 4 (1964) 36.
[41] M. G. Fontana, *Corrosion engineering*, Tata McGraw-Hill, New Delhi, India, 36 (2005) 1375-1379.
[42] S. Kalia, C. Processing: A study of materials at low temperatures, *J. Low Temp. Phys*, 158 (2010) 934-945.
[43] H. Yumoto, Y. Nagamine, J. Nagahama and M. Shimotomai, Corrosion and stability of cementite films prepared by electron shower, *Vacuum*, 65 (2002) 527-531.

Srinivasagam Ramesh is presently working as Teaching Fellow in the Department of Mechanical Engineering, Anna University, Chennai, India. He obtained his Master of Engineering from Alagappa Chettiar College of Engineering & Technology, Karaikudi, India. His field of research interests include corrosion, cryogenics treatments for materials, material characterization, and optimization.

B. Bhuvaneshwari worked as a Adhoc Scientist at CSIR- Structural Engineering Research Centre (CSIR- SERC), Chennai India and has more than 6 years of Research and Development experience. Her field of research interests include advanced composite materials, corrosion of metals, polymer synthesis and functional materials characterization. She has published more than 15 papers in various referred international and national journals, more than 40 papers in various Conference/Seminar/Workshop proceedings.

G. S. Palani is presently a Chief Scientist at CSIR-Structural Engineering Research Centre (CSIR-SERC), Chennai, India and has Research and Development experience of more than 25 years. His field of research interest include advanced finite element analysis, computational Structural dynamics, fatigue and fracture analysis, steel structures analysis, design & testing and material science. He has published over 60 papers in various refereed international and national journals, more than 110 papers in various Conference/Seminar/Workshop proceedings. He has 4 copyrights of software and 3 proceedings volumes to his credit.

D. Mohan Lal is currently a Professor at the Department of Mechanical Engineering, Anna University, Chennai, India. He has been working in the field of Refrigeration for the past 25 years and has guided many M.E. Theses and 12 Ph.Ds. He has published 63 research papers in international journals focusing on heat transfer characteristics of refrigerants, heat transfer in nanofluids, performance assessment of refrigeration system.

Nagesh R. Iyer is presently a Distinguished Professor in Academy of Scientific & Innovative Research (AcSIR) and former Director of CSIR-Structural Engineering Research Centre (CSIR-SERC), Chennai and the Coordinating Director of CSIR Madras Complex. He has over 35 years of experience in the areas of Computational Structural Mechanics, Fatigue, Fracture Mechanics, Damage Mechanics, Damage Tolerance, performance evaluation & condition monitoring of structures and Structure-Interaction studies. He has published over 130 papers in national & international journals, over 175 papers at the national & internal conferences and 4 patents.